Proceedings of the 21st ICSMGE, Vienna, Austria, 14 – 19 June 2026. Pistrol, Adam & Schweiger (eds.)
Published by: ÖGG, Austrian Society for Geomechanics, Salzburg, Austria, ISBN 978-3-9503898-4-5
https://doi.org/10.53243/ICSMGE2026-1181

High-fidelity multiscale framework for modelling permafrost thaw-related geohazards

Jidu Yu, Jidong Zhao
Dept of Civil and Environmental Engineering, Hong Kong University of Science and Technology, Kowloon, Hong Kong, China
jzhao@ust.hk

ABSTRACT: This paper presents a multiscale framework for modelling permafrost thaw-related geohazards. The framework integrates the material point method (MPM) for multiphysics large deformation modelling in the macroscale continuum-level and the discrete element method (DEM) for capturing complex, loading-dependent material responses of ice-rich granular soils. The macroscopic THM-coupled governing equations are formulated based on the mixture theory. An efficient hybrid explicit-implicit MPM algorithm is developed to alleviate timestep size dependence on changing permeability conditions in frozen soils. A simple ice saturation-dependent bond contact model is incorporated into the DEM solver to characterize the effects of ice cementation and its degradation due to ice melting and bond breakage. Two retrogressive thaw slump examples are simulated, demonstrating the framework's effectiveness in simulating thaw-related geohazards, with explainable underlying microscopic mechanisms. This framework offers a promising computational tool for understanding and predicting the freeze-thaw behaviour of granular media in cold regions.

KEYWORDS: Permafrost thaw, geohazard, thaw slump, THM coupling, multiscale modelling, MPM, DEM.

1 INTRODUCTION

Global warming is accelerating the thawing of permafrost in cold regions (Lewkowicz & Way 2019), triggering increasing natural disasters such as retrogressive thaw slumps (RTSs). Recent studies show that, from 2008 to 2012, the number of RTSs and the affected areas on the Qinghai-Tibet Plateau increased by 4 to 6 times, respectively (Luo et al. 2022). Permafrost thaw also triggers a series of other geotechnical and environmental hazards, including foundation subsidence, road cracking, bridge collapse, and contaminant dispersions (Figure 1). It is estimated that by 2050, 70% of infrastructure in permafrost regions will be at risks, with potential economic losses reaching billions of dollars (Hjort et al. 2022).

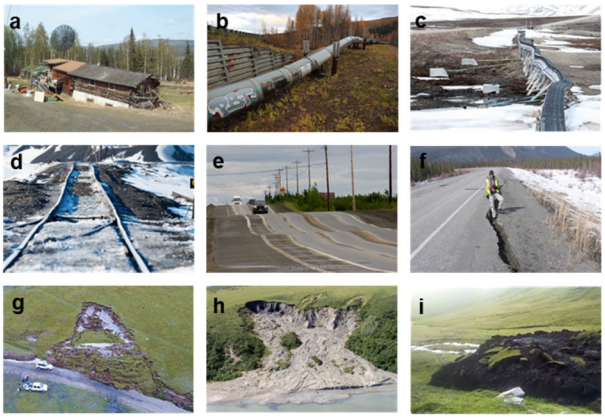

Figure 1 Typical infrastructure damage, geohazards, and thermokarst landscapes related to permafrost thaw. [Images sourced from website]

Despite growing research on the intensification of geohazards caused by permafrost thaw, advanced numerical tools for predicting and analysing thaw processes, underlying mechanisms, and impacts remain lacking. The challenges lie in three key aspects: (i) thawing permafrost involves ice-water phase transitions, with significant differences in material properties between frozen and unfrozen states, complicating constitutive modelling; (ii) permafrost is a multiphase granular medium whose mechanical behaviour is strongly coupled with thermal and hydraulic fields, requiring THM coupling tools for dynamic thaw simulation; (iii) ice-rich permafrost exhibits fluid-like behaviour post-thaw, necessitating numerical tools suited for large-deformation modelling.

Conventional FEM struggles to model thaw-related large deformations due to mesh distortion at large strain. In recent years, particle-based methods, such as MPM, have seen rapid development in modelling multiphysics large deformation problems in granular media (Soga et al. 2016; Yu et al. 2024a, 2025). Similar to FEM, MPM is a continuum-based method that relies on constitutive models to update the mechanical response of materials. However, the constitutive behaviour of frozen soil is highly complex, and existing models struggle to account for processes such as ice bond melting and breakage at the particle scale (Nishimura et al. 2009). Alternatively, the DEM can effectively capture the particle-scale responses of frozen soil (Chang et al. 2023). However, the high computational cost of DEM limits its use to large-scale engineering problems.

To address these gaps, we propose a multiscale MPM-DEM approach for modelling thaw-related problems. The MPM is used for THM-coupled large-deformation modelling at the macroscopic level, while the DEM is employed for update path- and history-dependent granular responses at the micro- and mesoscale, surpassing conventional phenomenological constitutive models (Liang et al. 2023; Yu et al. 2024b). Specifically, an ice saturation-dependent bond-based DEM model is developed to capture the permafrost degradation due to ice melting. Additionally, a hybrid explicit-implicit MPM algorithm is implemented to efficiently solve THM coupled problems. This method provides a new computational tool for investigating granular mechanics of permafrost soils and thaw-related geohazards in cold regions.

2 METHODOLOGY

We consider a frozen porous medium composed of soil grains (s), ice crystals (i), and liquid water (l), and assume: (A) all phases are uniformly distributed and can be described using the mixture theory; (B) soil particles are considered incompressible; (C) the ice and soil grains form solid skeleton together and jointly bear effective stress; (D) the flow of unfrozen water satisfies Darcy's law; (E) all phase temperatures are assumed equal, reflecting local thermodynamic equilibrium; and (F) the plastic heat generation is not considered. Based on these assumptions, we establish the macroscopic governing equations within the single-point multiphase MPM framework, with the effective stress of the ice-soil skeleton updated by DEM. The multiscale framework is detailed as follows.

2.1 *Macroscopic governing equations for frozen soil*

We adopt the $\boldsymbol{v}_s - \boldsymbol{v}_l - p_l - T$ formulation for the macroscale governing equations,, where $\boldsymbol{v}_s$ and $\boldsymbol{v}_l$ are the velocities of the solid and liquid phases, respectively, p_l is the pore liquid

pressure, and T is the temperature. It is important to note that, under the assumption (B), the velocity of ice is equal to that of the soil particles, both of which are equal to $\boldsymbol{v}_s$.

Based on this, the momentum balance equation for the multiphase mixture can be formulated as follows:

$$(n_s\rho_s + n_i\rho_i)\frac{d_s\boldsymbol{v}_s}{dt} + n_l\rho_l\frac{d_s\boldsymbol{v}_l}{dt} = \nabla\cdot\boldsymbol{\sigma} + \rho_m\boldsymbol{b}, \quad (1)$$

where $d_s(*)/dt$ is the material derivative of field $(*)$ regarding the solid phase; n_π and ρ_π are the volume fraction and intrinsic density of phase $\pi \in \{s, i, l\}$, respectively; ρ_m is the mixture density; $\boldsymbol{\sigma} = \boldsymbol{\sigma}'_{\mathrm{RVE}} - p_l\boldsymbol{m}$ is the total stress; $\boldsymbol{\sigma}'_{\mathrm{RVE}}$ is the effective stress; $\boldsymbol{m}$ is the identity tensor; and $\boldsymbol{b}$ is the body force. Besides, the flow of unfrozen water should satisfy:

$$n_l\rho_l\frac{d_s\boldsymbol{v}_l}{dt} = -n_l\nabla p_l + n_l\rho_l\boldsymbol{b} - n_l^2\frac{\rho_l g}{k_0 k_r}(\boldsymbol{v}_l - \boldsymbol{v}_s), \quad (2)$$

where k_0 is the absolute hydraulic conductivity; k_r is the relative hydraulic conductivity; and g is the gravitational acceleration.

Moreover, the mass conservation of frozen soil needs to account for the phase transition between ice and water, the variations in the densities of each phase caused by changes in temperature and pressure, as well as the effects of skeleton deformation and the migration of unfrozen water. The final equation is expressed as follows:

$$\zeta n\frac{d_sS_l}{dt} + \frac{n_l}{K_l}\frac{d_sp_l}{dt} - \beta_m\frac{d_sT}{dt} + (1-\zeta n_i)\nabla\cdot\boldsymbol{v}_s + \nabla\cdot n_l(\boldsymbol{v}_l - \boldsymbol{v}_s) = 0, \quad (3)$$

where $\zeta = 1 - \rho_i/\rho_l$ is the volumetric expansion coefficient of pore water on freezing; β_m is the mixture thermal expansivity; S_l is the liquid saturation; and K_l is the liquid bulk modulus.

In addition, the latent heat effect due to the ice melting should be considered in the energy balance equation, given by:

$$C_m\frac{d_sT}{dt} + n\rho_iL_f\frac{d_sS_l}{dt} + n_l\rho_lc_l(\boldsymbol{v}_l - \boldsymbol{v}_s)\cdot\nabla T + \nabla\cdot(-\kappa_m\nabla T) = Q, \quad (4)$$

where C_m and κ_m are the mixture heat capacity and thermal conductivity, respectively; L_f is the latent heat of fusion; and Q is the heat source.

In addition to these three fundamental conservation equations, a soil freezing characteristic curve (SFCC) that describes the relationship between liquid saturation with temperature and a hydraulic conductivity model related to porosity and ice saturation are also required. For details, please refer to our previous papers (Yu et al. 2024a, b).

2.2 *Discrete element model for ice-rich soil skeleton*

We use pure frictional contact as the basic contact model for particles without ice and employ bond contact to model the bonding effect when ice exists, as illustrated in Figure 2. Particle stiffness and bond strength are both dependent on ice saturation. For simplicity, we adopt the following relations:

$$C_\alpha = C_{\alpha 0} + \Delta C_\alpha^{max}\phi_{C\alpha}(S_i), \ \alpha = \eta, \tau, \quad (5)$$

$$E_c = E_{c0} + \Delta E_c^{max}\phi_E(i), \quad (6)$$

where η and τ represent the normal and tangential directions, respectively; $C_{\alpha 0}$ and E_{c0} are the cohesion strength and particle Young's modulus without ice bond; ΔC_α^{max} and ΔE_c^{max} are the maximum additional cohesion and Young's modulus due to ice bond; and $\phi_{C\alpha}$ and ϕ_E are functions related to ice saturation S_i. Since the bonding effect might be insignificant at low ice saturation, an *S-shaped* function is adopted for $\phi_{C\alpha}$ and ϕ_E:

$$\phi_{C\alpha} = \phi_E = 1 - (1 - {S_i}^m)^m, \quad (7)$$

where m is a shape parameter. In this study, the value of $m = 2$ is adopted. In addition, the grain size is updated based on the ice saturation and volumetric strain as follows:

$$r_{eq} \approx r_0\sqrt{\frac{1 - n_0 + (n_0 + \varepsilon_v)S_i}{1 - n_0}}, \quad (8)$$

where r_0 is the initial grain size; n_0 is the initial porosity; ε_v is the volumetric strain; and S_i is the ice saturation degree.

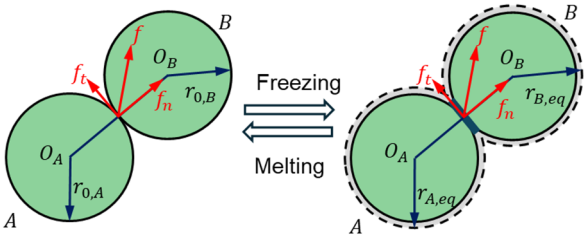

Figure 2 Illustration of DEM contact model.

2.3 *Multiscale MPM-DEM solution algorithm*

The multiscale framework is implemented by attaching an representative volume element (RVE) to each material point. The ice saturation obtained from the MPM solver is passed to the DEM solver to update the parameters within the RVE, while the displacement gradient is applied as the boundary condition for RVE shearing. The DEM solver then returns homogenized effective stresses and other mesoscale information such as porosity to facilitate MPM solution. RVEs retain their prior loading states at each incremental time step, allowing for loading history-dependent stress update. This capability is particularly important for modelling time-dependent freeze-thaw behaviour of granular media. The bidirectional information exchange between two scales is performed once during each MPM time step. To enable the use of larger time steps, we propose a hybrid explicit-implicit MPM scheme, which can significantly reduce the computational time required for the DEM solver compared to a fully explicit MPM approach.

Specifically, the nodal temperature is updated using the following explicit method:

$$\dot{T}_I^{k+1} = C_I^{-1}\left(e_I^{int} + e_I^{ext}\right), \quad (9)$$

while the nodal velocities are updated using the following node-based implicit method:

$$\begin{bmatrix}\dot{\boldsymbol{v}}_{sI}^{k+1}\\ \dot{\boldsymbol{v}}_{lI}^{k+1}\end{bmatrix} = \begin{bmatrix}M_{sI} & M_{lI}\\ -\Delta t Q_I^d & M_{lI} + \Delta t Q_I^d\end{bmatrix}^{-1}\begin{bmatrix}\boldsymbol{f}_{mI}^k\\ \boldsymbol{f}_{fI}^k\end{bmatrix}. \quad (10)$$

Here, C_I, e_I^{int}, e_I^{ext}, M_{sIl}, M_{lI}, Q_I^d, $\boldsymbol{f}_{mI}^k$, and $\boldsymbol{f}_{fI}^k$ are nodal coefficients and forces. In addition, the pore water pressure is computed on particle as follows:

$$\dot{p}_{lp}^{k+1} = -K_p^{-1}\left(K_T\dot{T}_p^{k+1} + K_s\dot{\varepsilon}_{vsp}^{k+1} + K_l\dot{\varepsilon}_{vlp}^{k+1}\right). \quad (11)$$

Here, K_p, K_T, K_s, are K_l are scalar coefficients, and $\dot{\varepsilon}_{vs}^{k+1}$ and $\dot{\varepsilon}_{vl}^{k+1}$ are the volumetric strain rate of solid and liquid phases, respectively. For the details of the coefficients in Eq. (9)~ Eq. (11), one may refer to Yu et al. (2024a, b).

The main solution procedure for the multiscale MPM-DEM approach is given as follows and illustrated in Figure 3.

1. Map mass, momentum, and energy information from MPs to the grid, then calculate the nodal velocities $\boldsymbol{v}_{sI}^k$ and $\boldsymbol{v}_{lI}^k$ and nodal temperature T_I^k.
2. Calculate the strain rate at the MPs, and update pore water pressure, water saturation, and ice saturation.

3. Calculate the displacement gradient $\nabla \boldsymbol{u}_p^k$. Then, transfer $\nabla \boldsymbol{u}_p^k$ and ice saturation S_{ip}^k to the DEM solver. update RVE properties and shear RVEs to obtain effective stress $\boldsymbol{\sigma}'_{\mathrm{RVE}}$.
4. Compute nodal internal and external forces, and heats using the updated MP information, and then compute nodal temperature rate $\dot{T}_I^{k+1}$ and accelerations $\dot{\boldsymbol{v}}_{sI}^{k+1}$ and $\dot{\boldsymbol{v}}_{lI}^{k+1}$.
5. Update MP velocities $\boldsymbol{v}_{sp}^{k+1}$ and $\boldsymbol{v}_{lp}^{k+1}$ and temperature T_p^{k+1}, as well as their displacement and coordinates.

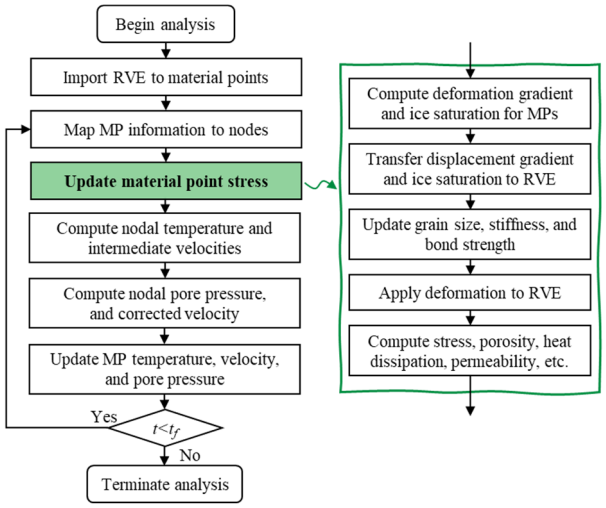

Figure 3 Overall solution procedure for MPM-DEM framework.

3 NUMERICAL EXAMPLES

3.1 *RVE preparation*

The RVE is generated using the bond contact model by setting a zero-bond strength, which is equivalent to a pure frictional contact model. The microparameters used for the RVE generation are given as follows: grain density ρ_{grain}=2650 kg/m^3, grain size r_{grain}=3~7 mm, Young's modulus E_c =0.6 GPa, Poisson's ratio, ν_c=0.8, and frictional coefficient μ=0.5. A relative dense RVE packing with an initial porosity of 0.18 is prepared under an isotropic confining stress of 100 kPa, as shown in Figure 4(a). The distribution of contact normal orientations is shown in Figure 4(b), indicating that the RVE is relatively isotropic packing. Additional parameters related to ice-saturation-dependent bond are given as follows: ΔE_c^{max}=3 GPa, C_{i0}=1 MPa, and ΔC_i^{max}=50 MPa.

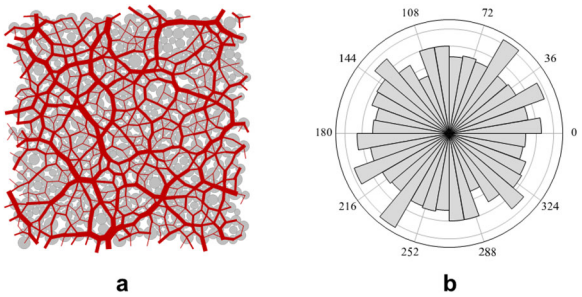

Figure 4 (a) The force chain of the RVE used for multiscale modelling, and (b) the rose diagram of the distribution of contact normal orientation of the RVE.

3.2 *Retrogressive thaw slump*

With global warming, retrogressive thaw slump (RTS) occurs more frequently in permafrost when an ice-rich section thaws (Armstrong et al. 2018). RTS develops quickly and can extend across several hectares, modifying landscapes significantly (Ramage et al. 2017). However, it is challenging to physically or numerically model the behaviour of RTS.

In this example, we simulate two slope failure cases caused by permafrost thaw. The geometry of the slope is shown in Figure 5. The left and bottom boundaries of the slope are assigned roller and fixed conditions, respectively. Both of them are impermeable and insulated boundaries. The initial temperature of the slope is set to -5 °C. The initial porosity of the slope is set to 0.4. A regular quadrilateral mesh is used as the background grid, with an element size of 0.2 m. Each element contains four material points. The material properties used for MPM modelling are given as follows: intrinsic density ρ_s=2650 kg/m^3, ρ_l=1000 kg/m^3, and ρ_i=910 kg/m^3; specific heat c_s =800 J/(kg·°C), c_l =4200 J/(kg·°C), and c_i =2060 J/(kg·°C); thermal conductivity κ_s =1.0 W/(m·°C), κ_l =0.6 W/(m·°C), and κ_i=2.2 W/(m·°C), and hydraulic conductivity k =1×10^{-4} m/s. To accelerate heat transfer, the thermal conductivity of all phases is scaled up by 8.64×10^5 s/d.

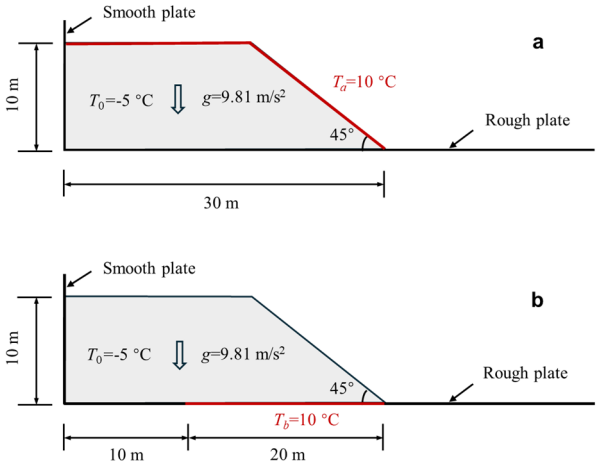

Figure 5 Model setups for the retrogressive thaw slump simulation: (a) Case I and (b) Case II.

In Case I, we simulate the progressive failure of a thawing slope caused by an increase in ambient temperature. Figure 6 illustrates the simulation results of ice saturation, deviatoric strain, and displacement during the thawing failure process. As the temperature increases, the frozen slope begins to thaw progressively from the surface toward the interior. The melting of ice in soils results in the loss of cementation between soil particles, leading to a reduction in strength and, consequently, triggering slope failure. It can be observed that as the thawing front progresses deeper, the slip surface gradually moves inward, and the overall failure behaviour exhibits a fluid-like flow pattern.

In Case II, we consider a thaw slump triggered by heating at the base of the slope. This scenario may occur in the presence of underground warm flow or geothermal activities. For demonstration purposes, we simply set part of the slope base temperature to be 10°C, as depicted in Figure 5b. The simulation results are shown in Figure 7. Unlike Case 1, in this case, the slope thaws from the bottom toward the upper part. Due to the loss of support at the bottom, a weakened base layer forms, leading to the development of an inclined shear band that extends to the top surface of the slope and ultimately causes the slope's global failure. In addition, we examined the RVEs at two points in the shear band: point A, located in the unfrozen region (Figure 7a), and point B in the thawed region (Figure 7b). It was observed that both RVEs experienced significant shear deformation. At Point A, lots of bond breakage occurred under deformation, while at Point B, all ice bonds are lost due to complete melting. Therefore, the proposed multiscale approach

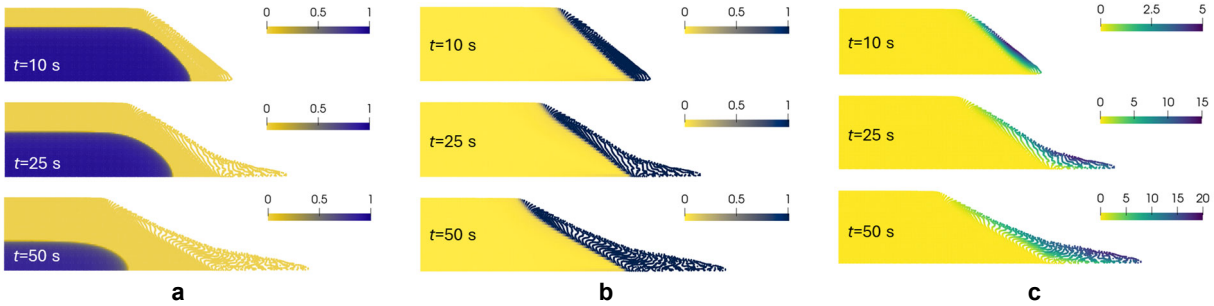

Figure 6 Simulation results of (a) ice saturation S_i, (b) deviatoric strain ε_d, and (c) displacement magnitude $|\boldsymbol{u}|$ in Case I at different elapsed times.

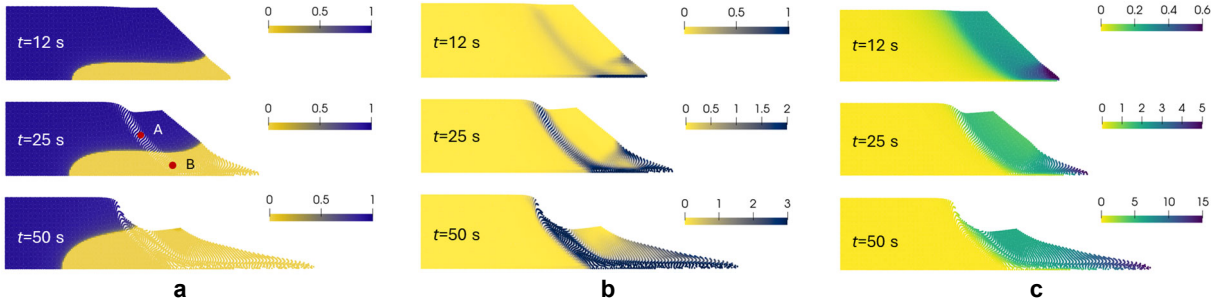

Figure 7 Simulation results of (a) ice saturation S_i, (b) deviatoric strain ε_d, and (c) displacement magnitude $|\boldsymbol{u}|$ in Case II at different elapsed times.

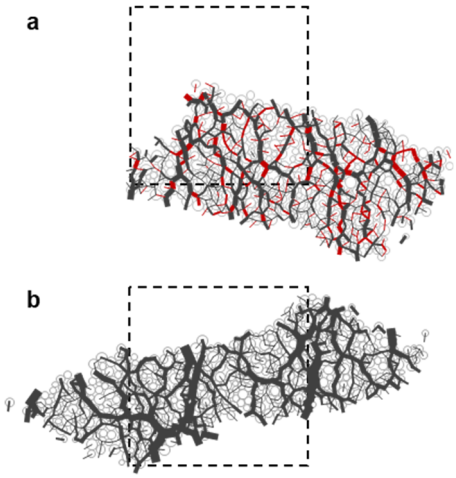

Figure 8 Force chain of selected RVEs. Red line – intact bond; black line – broken bond, non-ice bond, or pure frictional contact.

effectively captures the melting and breakage of ice bonds during the thawing and shearing processes in permafrost from a microscopic perspective, providing a more physics-based simulation compared to conventional constitutive models.

4 CONCLUSIONS

This paper presents a multiscale MPM-DEM framework for simulating geohazards caused by permafrost thaw. A bond-based DEM is employed to update the effective stress of soils during thawing, while the MPM is used to solve the macroscopic THM-coupled large deformation responses. Through two thaw slump simulations, we demonstrate that the method can effectively simulate thaw-related geohazards with explainable underlying microscopic mechanisms. Future work should be focused on refining the DEM model and carefully calibrating the microscopic parameters based on experimental data to enable simulations for more realistic scenarios.

5 ACKNOWLEDGEMENTS

This work is financially supported by National Natural Science Foundation of China (Project No. 11972030), Research Grants Council of Hong Kong (GRF #16212724, RIF #R6008-24, and TRS #T22-607/24N and #T22-606/23R).

6 REFERENCES

Armstrong, L., Lacelle, D., Fraser, R.H., Kokelj, S., and Knudby, A. 2018. Thaw slump activity measured using stationary cameras in time-lapse and Structure-from-Motion photogrammetry. *Arctic Science* 4, 827–845.

Chang, D., Yan, Y., Liu, J., Xu, A., Feng, L., and Zhang, M. 2023. Micro-macroscopic mechanical behavior of frozen sand based on a large-scale direct shear test. *Computers and Geotechnics* 159, 105484

Hjort, J., Streletskiy, D., Dor´e, G., Wu, Q., Bjella, K., and Luoto, M. 2022. Impacts of permafrost degradation on infrastructure. *Nature Reviews Earth & Environment* 3, 24–38.

Lewkowicz, A.G., and Way, R.G. 2019. Extremes of summer climate trigger thousands of thermokarst landslides in a High Arctic environment. *Nature Communications* 10, 1329.

Liang, W., Zhao, J., Wu, H., and Soga, K. 2023. Multiscale, multiphysics modeling of saturated granular materials in large deformation. *Computer Methods in Applied Mechanics and Engineering* 405, 115871.

Luo, J., Niu, F., Lin, Z., Liu, M., Yin, G., and Gao, Z. 2022. Inventory and Frequency of Retrogressive Thaw Slumps in Permafrost Region of the Qinghai–Tibet Plateau. *Geophysical Research Letters* 49, e2022GL099829.

Nishimura, S., Gens, A., Olivella, S., and Jardine, R.J. 2009. THM-coupled finite element analysis of frozen soil: Formulation and application. *Geotechnique* 59, 159–171.

Yu, J., Zhao, J., Liang, W., and Zhao, S. 2024a. Multiscale modeling of coupled thermo-hydro-mechanical behavior in ice-bonded granular media subject to freeze-thaw cycles. *Computers and Geotechnics* 171,1254.

Yu, J., Zhao, J., Zhao, S., and Liang, W. 2024b. Thermo-hydro-mechanical coupled material point method for modeling freezing and thawing of porous media. *International Journal for Numerical and Analytical Methods in Geomechanics* 48, 3308–3349.

Yu, J., Zhao, J., Liang, W., and Zhao, S. 2024c. A semi-implicit material point method for coupled thermo-hydro-mechanical simulation of saturated porous media in large deformation. *Computer Methods in Applied Mechanics and Engineering*, *418*, 116462.

Yu, J., Liang, W., and Zhao, J. 2025. Enhancing dynamic modeling of porous media with compressible fluid: A THM material point method with improved fractional step formulation. *Computer Methods in Applied Mechanics and Engineering*, *444*, 118100.